PHYSICAL REVIEW B VOLUME 26, NUMBER 6 15 SEPTEMBER 1982

Systematic approach for comparing paraelectric tunneling models to resonance data

Robert John Russell*
Physics Department, Carleton College, Northfield, Minnesota 55057
and Physics Board of Studies, University of California, Santa Cruz, California 95064
(Received 28 January 1982)

In paraelectric systems, reorientable impurity dipoles can give rise to resonance absorption of microwaves at liquid-helium temperatures. Several current models exist to explain paraelectricity in terms of tunneling between neighboring dipole orientations. In this paper we divide tunneling parameter space into several regions in which the effects of an additional electric field dependence facilitates data analysis of paraelectric resonance spectra. We give results for the two standard dipole models and for two field orientations, producing 32 multiple-energy-level diagrams and sum rules. These diagrams and sum rules greatly facilitate data analysis and allow a strong test of the theory.

INTRODUCTION

Finite-group theory plays a central role in the study of molecules and crystals. In 1965 a new area in solid-state physics opened in which group theory is particularly applicable, when tunneling centers were discovered in doped alkali-halide crystals.[1] These centers are formed by monatomic or molecular impurities which produce reorientable electric dipoles in the host crystal at a vacancy site. Typically the dipole orientation is restricted by a strong crystal potential to specific sets of equivalent directions. Reorientation, however, can occur by a temperature-independent tunneling process at rates up to $10^{+10}\ s^{-1}$, producing a multiplet of tunneling-split energy levels. The impurity centers carry an electric dipole moment $\vec{p}$ which can couple to an external dc electric field $\vec{E}_{dc}$ via a $-\vec{p}\cdot\vec{E}$ interaction.[2] The combination of the tunnel splittings and the electric field interaction produces effects, including resonance absorption, which are quite similar to those in paramagnetism; by analogy, this new field is called paraelectricity.

Among the dozen experimental techniques used in paraelectric research, microwave spectroscopy typically provides the most complete characterization of the paraelectric species, since in principle and for fast tunneling systems,[3] all of the important parameters of the existing tunneling models can be extracted from the data. In the past, however, such a complete characterization has been hampered on two accounts: Lack of *broadband* data and lack of an *efficient* method for exhaustively obtaining the best fit of the model to the data.

Recently with the development in our lab of an extremely broadband spectrometer (8—216 GHz, 0—150 kV/cm),[4] a wealth of data has been discovered on several new and complicated paraelectric systems. The quality and quantity of this new data has triggered the need for a much more precise fit with the existing models, the results of which could provide a critical test of these models.

We now report the development of a systematic method utilizing finite-group theory by which a small number of sets of parameters can be obtained which *necessarily* includes the *best* possible fit to the data. If these results are poor, one has effectively tested the *model,* since one knows in principle by this method that there can be *no* better fit under the existing assumptions of the test. Hence the potential power of the paraelectric resonance data now available may be engaged in a strong test of existing paraelectric theory.

TUNNELING MODELS IN PARAELECTRICITY

One of the most successful models used in paraelectricity was developed in 1966—1967 when Gomez, Bowen, and Krumhansl[5] (GBK) and others[6] extended Hund's double harmonic oscillator tunneling model to the cubic symmetry of the alkali-halide crystals. In the GBK model, the potential multiwell is composed of n equivalent simple harmonic oscillator wells formed by the host crystal at the defect site, and represented by a tun-

neling crystal-field Hamiltonian H_c. The wells lie along either the six $\langle 100\rangle$, the eight $\langle 111\rangle$, or the 12 $\langle 110\rangle$ crystal directions. The sets of states localized in these well form six-, eight-, and 12-fold-degenerate-directed state bases for H_c.[5] With finite barriers between wells, directed states in different wells overlap slightly, and tunneling between wells produces a tunneling-split multiplet. Following GBK, we use η, μ, ν, and σ to represent the matrix elements for tunneling to nearest-, second-nearest-, third-nearest-, and fourth-nearest-neighbor wells, respectively. Each tunneling eigenstate is characterized by the irreducible representation according to which it transforms, such as A_{1g}, T_{2u}, etc., where we follow standard group theoretic notation.[7] These eigenstates and their eigenvalues are easily obtained from group theory.[5] Differences between eigenvalues are called zero-field splittings (ZFS), since they occur in the absence of external electric fields.

A paraelectric salt can be strongly polarized by a $-\vec{p}\cdot\vec{E}_{dc}$ interaction with an external dc electric field, $\vec{E}_{dc}$. As the field is turned on, the cubic symmetry of the defect center is broken, and new eigenstates of the total Hamiltonian H_c+H_E form. In the simplest case, the application of the external field lowers the symmetry of the impurity from O_h to C_{4v}, C_{3v}, or C_{2v} as the field is applied parallel to either the $\langle 100\rangle$, the $\langle 111\rangle$, or the $\langle 110\rangle$ crystal directions, respectively. The levels usually move at first quadratically (as the net dipole moment of the eigenstates of H_c+H_E emerges) and then linearly in the applied field. Sets of directed states which lie in planes perpendicular to the applied field remain degenerate with respect to the $-\vec{p}\cdot\vec{E}$ interaction; remnant tunneling between states in these planes continues to lift their dengeneracy slightly. Hence energy levels that move together at high fields usually carry a fine tunneling structure imposed on the linear electric field effect[8] [Fig. 1(a)].

PARAELECTRIC RESONANCE

Paraelectric resonance (PER) is a highly sensitive technique for studying the spectrum of a paraelectric impurity.[9] Samples are mounted in a multimode microwave cavity at liquid-helium temperatures, and $\vec{E}_{dc}$ is applied parallel to either the $\langle 100\rangle$, $\langle 111\rangle$, or $\langle 110\rangle$ crystal axes. The microwave electric field $\vec{E}_{rf}$ is usually applied parallel to the dc field, so that resonance transitions correspond to allowed electric dipole transitions of the types: $A_1\rightarrow A_1$, $B_1\rightarrow B_1$, $B_2\rightarrow B_2$, and $E\rightarrow E$. Microwave absorption is recorded at a given frequency and temperature as the external electric field is swept through resonance. Each of these traces typically displays several absorption lines.[10] Finally, a composite graph of the compiled data for a given field orientation is constructed with frequency as the abscissa and field as the ordinant. At high fields, these lines display the asymptotic linearity of their energy levels, and their slopes are termed "high" and "low" as indicated in Fig. 1(b).

PREVIOUS PROCEDURES FOR FITTING THE MODEL

In the past, no rigorous algorithm existed for fitting the models to the PER data. One might be able to argue *against* one or more dipole models by some general observations: the number of ZFS's found in the data, the number of sets of resonance lines with different slopes, and the ratios of these

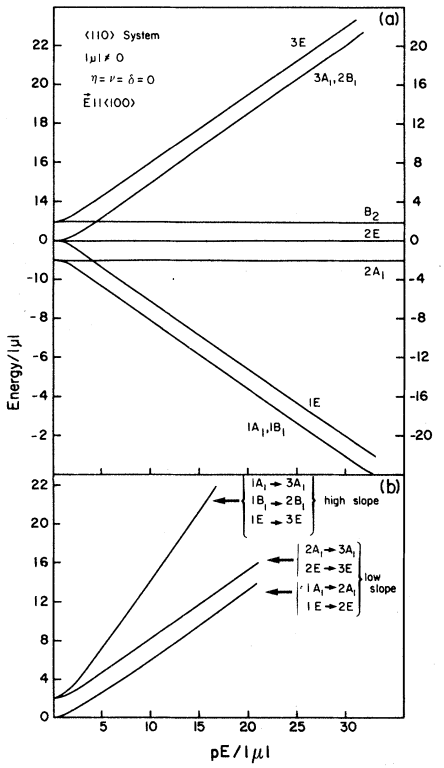

FIG. 1. Electric field dependence of the energy levels of a $\langle 110\rangle$ system is shown in part (a) for $\mu\neq 0$; $n=\nu=\sigma=0$. Notice the linearity of the dependence at high fields. Resonance transitions (allowed lines only) are shown in (b) for $\vec{E}_{rf}\|\vec{E}_{dc}$ where the field dependence is graphed against energy.

slopes in different field orientations.[11] However, these considerations are complicated by several problems. First of all, arguments based on the absence of ZFS's are contingent on the possibility that several such splittings may be degenerate; missing in the data (when the transition matrix elements are too small); at frequencies above the spectrometer band; or poorly resolved (due to line broadening). Next, lines that vary little with electric field are *quite* hard to detect. Finally, the comparison of slopes in the high-field limits of different field orientations does *not* in all cases give unambiguous results, as the same ratio of slopes can in some cases occur in more than one dipole model.

The problem of fitting a given model can also be considerably protracted if the data are extensive and complex, or alternatively if so few lines have been seen that many equally feasible alternative fits are possible. One might start by assuming that a given tunneling parameter should be dominant, with the choice being based on theoretical grounds or on evidence from other paraelectric experiments. However, there are no strong general theoretical grounds for the choice of the dominant tunneling parameter: GBK considered two different extremes of the harmonic potential well and found that either η or σ could dominant. Early experiments on RbCl:Ag^+ suggested that the system was $\langle 111 \rangle$ with η dominant; yet Lüty argued that it was a $\langle 110 \rangle$ system with μ dominant instead.[12]

Hence, one often begins by inspecting the gross features of the data, attempting to identify the dominant parameter(s) empirically. For example, the ratio of the relative intensities of the strong lines at high fields can be compared to perturbation calculations to suggest which parameters are largest. However, this can be misleading, since relative intensities depend on experimental parameters which are hard to measure accurately. Often, too, data cannot be obtained at high enough frequency for all lines to be in the high-field limit, as when larger splittings are involved.

Next, a numerical search may be made for sets of tunneling parameters which match the experimental zero-field splittings. If all the splittings have been seen in the data, this procedure can be fruitful, although its details still depend on which of the three tunneling models one uses. The numerical search we tried using the $\langle 110 \rangle$ model was especially time consuming, since halving the search increment lengthens the total search time by a factor of 16. Still the final, unavoidable problem with *any* numerical search is finite-mesh size: One is never certain that the *best possible* fit has actually been obtained after a given search.

Numerical solutions of the *total* Hamiltonian $H_c + H_E$ can then be pursued. For a given dipole model, electric field orientation, dipole moment (obtained asymptotically from the high-field spectra and the model assumed), and a given set of tunneling parameters, we numerically generated a plot of the theoretical resonance spectra, scaled to coincide with the composite graph of the experimental data, allowing direct visual comparison. Relative intensities were also tabulated for $T = 4.2$ and 1.3 K.

In our research[9] on the paraelectric species KBr:Li^+, approximately 100 such plots were produced from sets of tunneling parameters which had been found to match the splittings in the data to within our experimental resolution. Unfortunately, even small (1%) changes in a given tunneling parameter often produced enormous changes in several lines in the theoretical spectrum. Without a systematic basis for meticulously adjusting the parameters, the resulting search was almost random. In working with KBr:Li^+, the results of months of computer work were particularly unrewarding and inconclusive.

Hence, a systematic method was needed by which the choice of tunneling parameters could be obtained. The method should make *no* prior assumptions regarding which tunneling parameter is to be dominant, but should treat each parameter on an equal basis allowing for positive as well as negative values for the tunneling parameters.[13] The method should be efficient and practical. It necessarily includes certain assumptions about the data.[14] However, within these assumptions, it should enable one to identify a small set of possible tunneling parameters which *necessarily* includes the best possible fit for the model to the data.

NEW METHOD: MULTIPLE ENERGY-LEVEL DIAGRAMS

The method I now present uses multiple energy-level diagrams[15] in which the spectra for $\vec{E} \| \langle 100 \rangle$ and $\vec{E} \| \langle 111 \rangle$ are *jointly* displayed for all possible arrangements of the *zero-field* energy levels in all three dipole models. The power of this method arises from two observations: (a) For each such diagram, there is a distinct scheme by which the energy levels at zero field evolve into those at high fields, and hence a unique set of characteristics for the resulting resonance transition spectra; (b) for

each such diagram, there are continuous sets of values of each tunneling parameter for which the order of the zero-field energies, and hence the characteristics of the connection scheme to high fields, is invariant.

Hence, though one thinks of the tunneling parameters as determining the characteristics of the resonance data, one can equivalently think of the discrete arrangements of the zero-field energy levels as the determining factor, thereby transforming the problem from finding the values of several continuous variables with few analytic tools available to one of finding the most appropriate diagram out of a small set (32) of such diagrams.

In particular, the data can now be analyzed by comparing them to the diagrams, noticing the slopes of the allowed and forbidden lines at high fields and the manner in which they connect to the ZFS's, looking for sum rules among these ZFS's and checking for them in the data, and so on. Normally, there are at most only two or three choices for assigning the observed ZFS's to the theoretical splittings per diagram. Since one is simultaneously employing the spectra for two different field orientations, the number of such qualitative fits is minimized because the data must now be simultaneously consistent with *two* different field orinetations which share the *same* zero-field ordering. Once the best qualitative fits have been found, the tunneling parameters can be obtained algebraically[5] from the sizes of the ZFS's. Using the values of the tunneling parameters thus found, the full theoretical spectra can be numerically generated and compared with the data. We now know that within a given diagram no simple adjustment of the parameters will significantly change the overall fits since the parameters have been optimized algebraically already. The set of such fits therefore necessarily includes the best possible fit to the data.

In order to construct the multiple energy level diagrams, we must make two assumptions: (1) that the A_{1g} zero-field eigenstate has the lowest energy,[16] and (2) that no two energy levels, characterized by the same irreducible representation, may cross when $E \neq 0$. From (1) it follows that for m zero-field energy levels, there are $(m-1)!$ ways in which the levels can be ordered. Since there are two tunneling parameters for the $\langle 100 \rangle$ there must be two independent zero-field splittings and hence three zero-field energy levels. Thus there are only two different diagrams for the $\langle 100 \rangle$ model. For the $\langle 111 \rangle$ model with three tunneling parameters, there are four energy levels and hence six possible diagrams. For the $\langle 110 \rangle$ model with four tunneling parameters, there are five energy levels and hence 24 possible diagrams. Using (2), it follows that, for each possible ordering of the zero-field energies, there exists a unique scheme for connecting them to the available energy levels at high fields. We obtain this scheme from the decomposition rules for each energy eigenstate as the O_h symmetry is lowered by $\vec{E}_{dc}$, and from the symmetry of the available eigenstates at high fields. The complete set of 32 diagrams is given in Fig. 2.

As an example, consider the $\langle 110 \rangle$ dipole system with $\vec{E}_{dc} || \langle 100 \rangle$. As $\vec{E}_{dc}$ is applied, the cubic symmetry of the zero-field eigenstates is reduced to C_{4v}, and the five states decomposed into nine states as:

$$A_{1g} \rightarrow A_1, \quad E_g \rightarrow A_1 \oplus B_1, \quad T_{1u} \rightarrow A_1 \oplus E,$$

$$T_{2g} \rightarrow B_2 \oplus E, \quad T_{2u} \rightarrow B_1 \oplus E \ .$$

(In Table I the complete set of decompositions for each dipole model and each field orientation is given.) At high fields, the available energy levels are arranged in three distinct groups: two, composed of A_1, B_1, and E states, vary as $\pm pE/\sqrt{2}$, while the third, composed of A_1, B_2, and E states, remains unaffected by $\vec{E}_{dc}$. Now all nine levels produced by the decomposition of the zero-field states must connect with these nine available levels at high field. By assumption (2) there exists a unique set of such connections for a given ordering of the five zero-field energies.

Sum rules between the ZFS's also exist. For example, in diagram 2 of the $\langle 110 \rangle$ system, the transition E_g to $T_{1u}(ad)$ equals the sum of the transition E_g to $T_{2u}(ab)$ plus the transition T_{2u} to $T_{1u}(bd)$.

Along with interesting features particular to each of the 32 diagrams, there are several general features for each model which deserve special attention. Assuming in general the lack of accidental degeneracies,[17] we observe that for $\langle 100 \rangle$ *dipoles* with two tunneling parameters, three zero-field energy levels, three ZFS's, and two diagrams:

(1) In both diagrams, all three ZFS's are allowed splittings in the $\langle 100 \rangle$ regime ($\vec{E} || \langle 100 \rangle$), with sum rules among them in both cases.

(2) The largest ZFS also occurs as an allowed splitting in the $\langle 111 \rangle$ regime in diagram 1.

(3) All allowed transitions in both diagrams and in both $\langle 100 \rangle$ and $\langle 111 \rangle$ regimes are singlets in the following sense. Each ZFS is connected to, at most, one allowed line. Doublets (two lines with

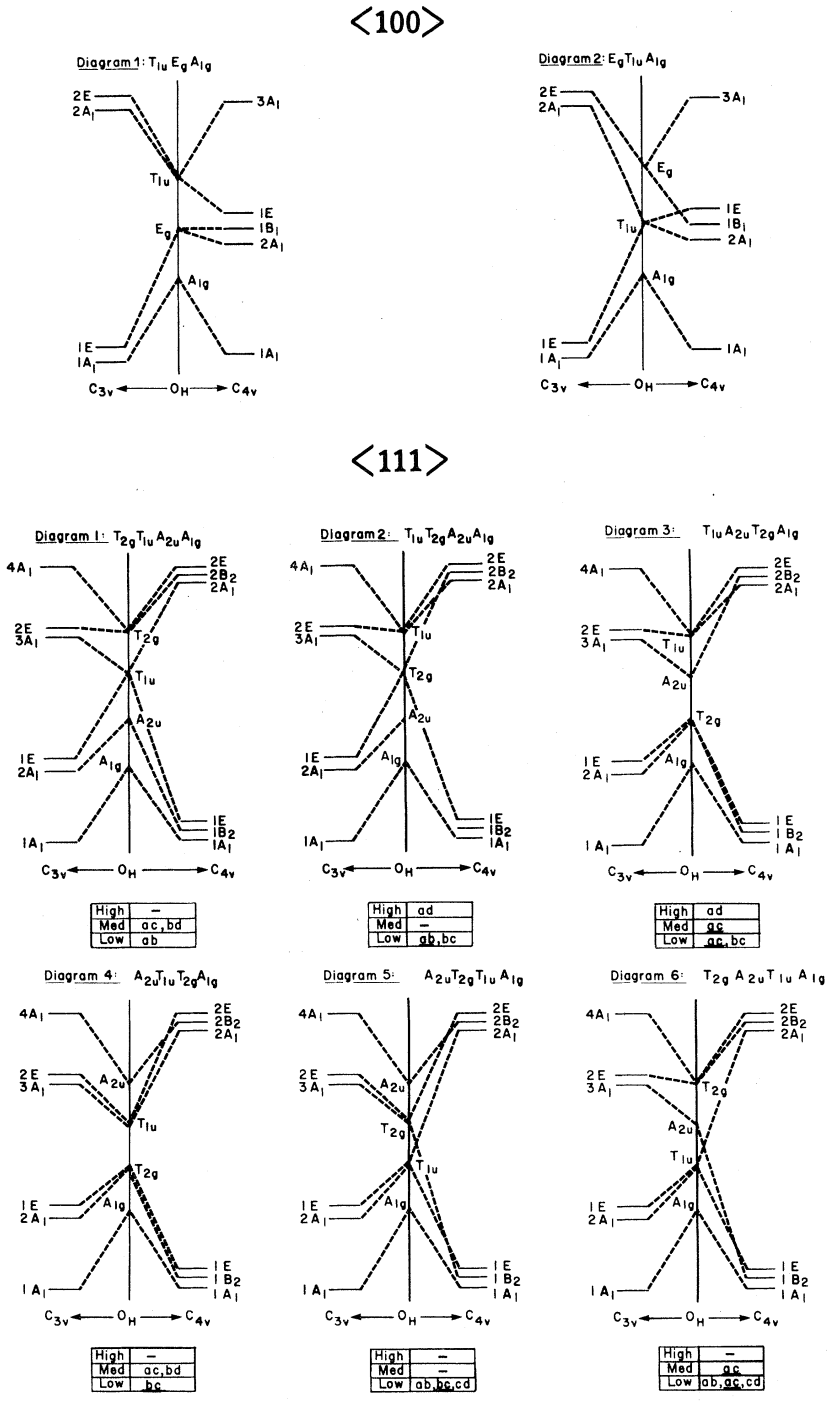

FIG. 2. 32 multiple diagrams are catagorized by the three types of standard tunneling models, ⟨100⟩, ⟨111⟩, and ⟨110⟩. In each diagram we join the spectra for $\vec{E}||\langle 100\rangle$ (C_{4v}) with that for $\vec{E}||\langle 111\rangle$ (C_{3v}) according to the order of the zero-field energies. To simplify notation, we label the zero-field energy levels *a* to *d* from top to bottom in the ⟨111⟩ system and *a* to *e* (from top to bottom) for the ⟨110⟩ system. Sum rules between ZFS's of allowed transitions are given for each diagram. In addition, ZFS's which join allowed transitions in both ⟨100⟩ and ⟨111⟩ are indicated in a box. ZFS's that connect to two allowed lines for a given field orientation are underlined (e.g., transition *cd* in diagram 1 of the ⟨110⟩ model).

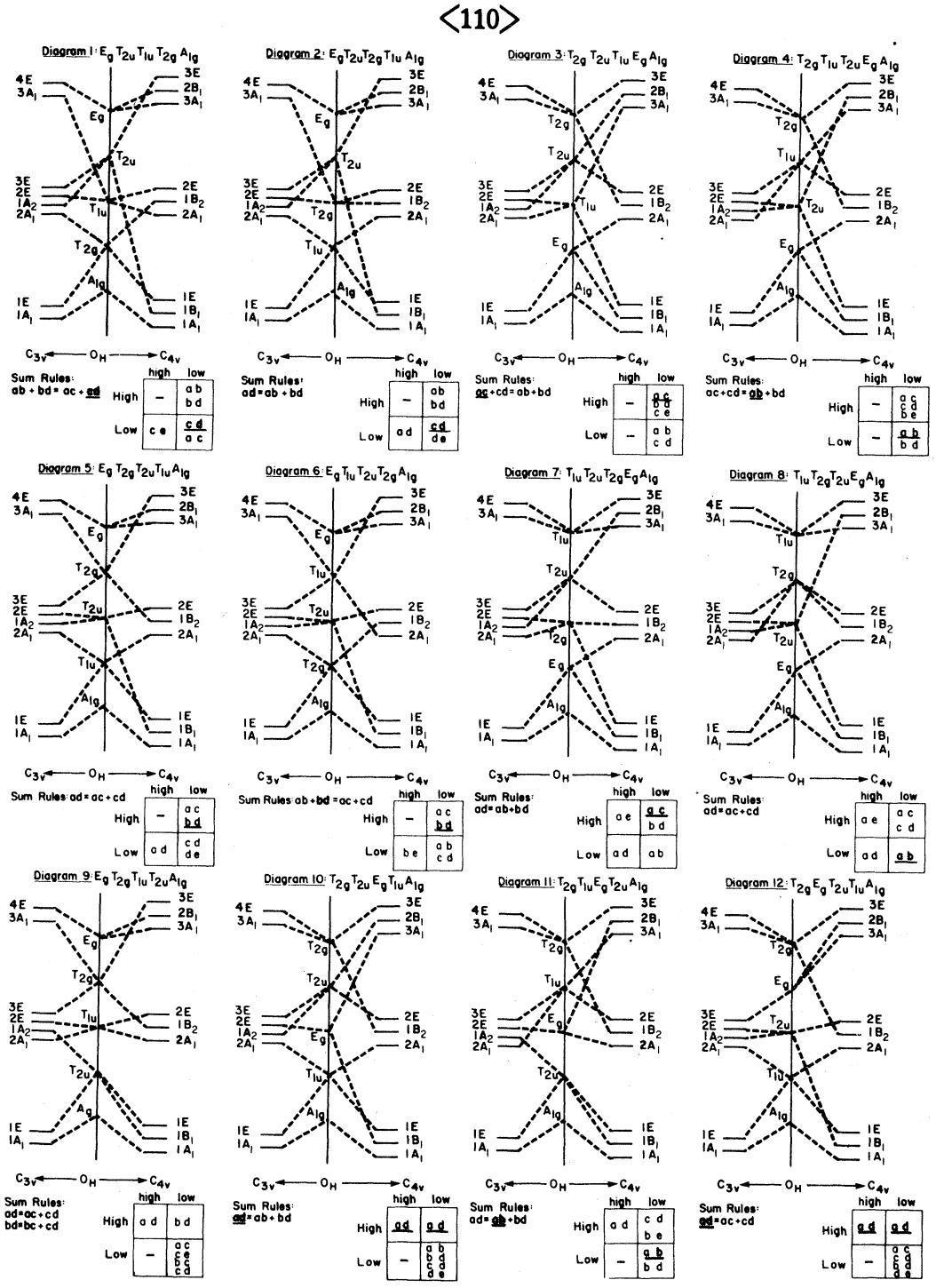

FIG. 2 (*Continued.*)

the same ZFS) may only occur if strain-allowed transitions are considered.

For ⟨*111*⟩ *dipoles* with three tunneling parameters, four zero-field energy levels, six ZFS's, and six diagrams:

(1) Sum rules occur in all six diagrams for the

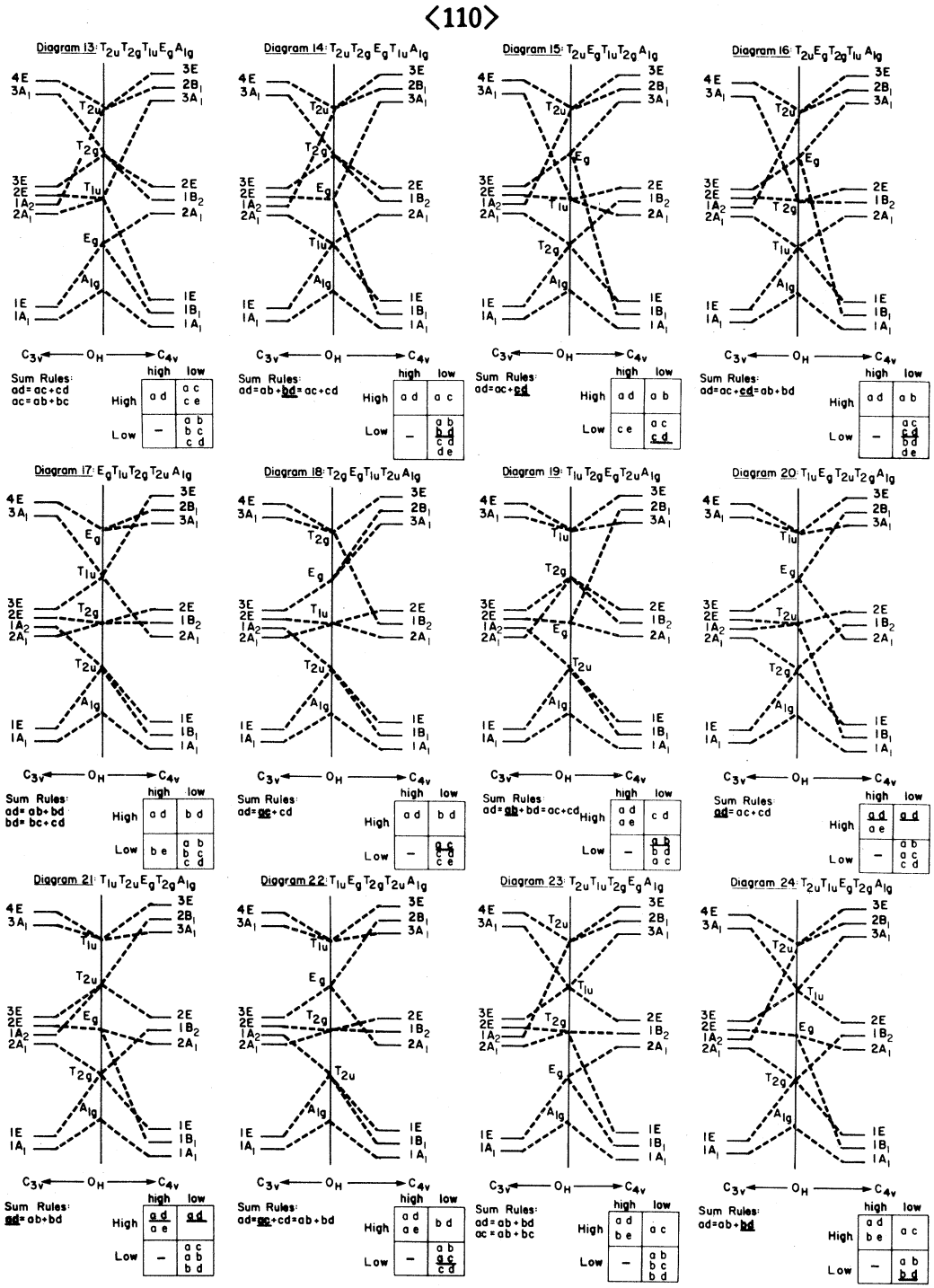

FIG. 2. (*Continued.*)

allowed ⟨111⟩ transitions. No sum rules occur in any of the diagrams in the allowed ⟨100⟩ transitions.

(2) In all six diagrams, all six ZFS's are allowed ⟨111⟩ transitions. Hence, no new ZFS's are found in the ⟨100⟩ transitions, even including forbidden transitions. The largest splitting is an allowed ⟨100⟩ transition only in diagrams 2 and 3.

TABLE I. Decomposition of eigenstates of O_h symmetry into eigenstates of C_{4v}, C_{3v}, and C_{2v} symmetry for the $\langle 100\rangle$, $\langle 111\rangle$, and $\langle 110\rangle$ dipole models, respectively.

O_h	→	C_{4v}	C_{3v}	C_{2v}
$\langle 100\rangle$				
A_{1g}	→	A_1	A_1	A_1
E_g	→	$A_1 \oplus B_1$	E	$A_1 \oplus B_1$
T_{1u}	→	$A_1 \oplus E$	$A_1 \oplus E$	$A_1 \oplus B_1 \oplus B_2$
$\langle 111\rangle$				
A_{1g}	→	A_1	A_1	A_1
A_{2u}	→	B_2	A_1	B_2
T_{1u}	→	$A_1 \oplus E$	$A_1 \oplus E$	$A_1 \oplus B_1 \oplus B_2$
T_{2g}	→	$B_2 \oplus E$	$A_1 \oplus E$	$A_1 \oplus A_2 \oplus B_2$
$\langle 110\rangle$				
A_{1g}	→	A_1	A_1	A_1
E_g	→	$A_1 \oplus B_1$	E	$A_1 \oplus B_1$
T_{1u}	→	$A_1 \oplus E$	$A_1 \oplus E$	$A_1 \oplus B_1 \oplus B_2$
T_{2g}	→	$B_2 \oplus E$	$A_1 \oplus E$	$A_1 \oplus A_2 \oplus B_2$
T_{2u}	→	$B_1 \oplus E$	$A_2 \oplus E$	$A_1 \oplus A_2 \oplus B_1$

For each diagram the allowed transitions for $\vec{E}||\langle 100\rangle$ and $\vec{E}||\langle 111\rangle$ that have the *same* ZFS's are tabulated in a box at the bottom. *The zero-field states are labeled a, b, c, and d starting with a at the top* and the three types of slopes for $\vec{E}||\langle 111\rangle$ are labeled by the transitions at high-E field (see Fig. 2). High denotes a transition from the lowest state to the highest, medium denotes a transition from the lowest to the second-highest group of states or from the second-lowest group to the highest, and low denotes transitions between neighboring groups of states. For example, in diagram 1, there is no allowed $\vec{E}||\langle 100\rangle$ line that has the same ZFS as the *high*-slope $\langle 111\rangle$ line. There is one ZFS that joins both to a *low*-slope $\langle 111\rangle$-allowed line and a $\langle 100\rangle$-allowed line—the *ab* splitting ($T_{2g}-T_{1u}$). Two *medium*-slope $\langle 111\rangle$ lines ($4A_1 \leftrightarrow 2A_1, 3A_1 \leftrightarrow 1A_1$) are joined to allowed $\langle 100\rangle$ lines ($2B_2 \leftrightarrow 1B_2, 2A_1 \leftrightarrow 1A_1$) through the ZFS *ac* ($T_{2g}-A_{2u}$) and *bd* ($T_{1u}-A_{1g}$), respectively.

For $\langle 110\rangle$ *dipoles* with four tunneling parameters, five zero-field energy levels, 10 ZFS's, and 24 diagrams:

(1) In the $\langle 100\rangle$ regimes of all diagrams, there are only seven allowed lines, all of which are *singlets*: No two allowed lines for $\vec{E}||\langle 100\rangle$ may share the same ZFS. Only seven of the 10 possible ZFS's can occur in the $\langle 100\rangle$ data as allowed lines.

(2) In the $\langle 111\rangle$ regimes of all diagrams, there are only eight allowed lines. In some cases, all eight lines are singlets; in other cases, two of them must arise from the same ZFS. If the T_{2g} and T_{1u} eigenstates are the second- and third-largest eigenstates (in either order), then all eight lines are singlets. In this case, two of the 10 ZFS's are not allowed in the $\langle 111\rangle$ data. If this condition is not met, then the $T_{1u}-T_{2g}$ splitting is a doublet, and three splittings cannot occur in the $\langle 111\rangle$ data. Thus, the *only* (allowed) doublet ZFS's occurs as the $T_{1u}-T_{2g}$ splitting in the $\langle 111\rangle$ data.

(3) In all diagrams, at least one (the $A_{1g}-T_{2u}$), and in some cases two (the $A_{1g}-T_{2u}$ and E_g-T_{2g}), of the ten ZFS's are *not* allowed in *either* the $\langle 100\rangle$ *or* the $\langle 111\rangle$ spectrum.

These remarkable conclusions arise from the following arguments (cf. Fig. 2). In the $\langle 100\rangle$ regimes of all diagrams, no allowed lines arise from the following three splittings: $A_{1g}-T_{2u}$, $A_{1g}-T_{2g}$, E_g-T_{2g}. In the $\langle 111\rangle$ regimes of all diagrams, no allowed lines arise from the following two splittings: $A_{1g}-T_{2u}$, $A_{1g}-E_g$. In addition, when eigenstates T_{2g} and T_{1u} are not the second- and third-largest eigenstates (in either order), then an additional ZFS is not seen in the data. That ZFS is the transition between second- and third-largest eigenstates, for which there are five possibilities: $T_{1u}-T_{2u}$ (diagrams 1, 3, 4, and 6), $T_{1u}-E_g$ (diagrams 11, 15, 18, and 24), $T_{2g}-T_{2u}$ (diagrams 2, 5, 7, and 8), $T_{2g}-E_g$ (diagrams 14, 16, 19, and 22), or $T_{2u}-E_g$ (diagrams 10, 12, 20, and 21). Hence, in all diagrams, the $A_{1g}-T_{2u}$ splitting is not seen in either the $\langle 100\rangle$ or $\langle 111\rangle$ data, and in those diagrams (14, 16, 19, and 22) in which the T_{2g} and E_g eigenstates are second and third largest, the $T_{2g}-E_g$ splitting is also not seen in either the $\langle 100\rangle$ or $\langle 111\rangle$ data.

(4) In every diagram there is at least one, and in many cases several, sum rules among the *allowed* ZFS's. The number of sum rules in each diagram is such as to leave only four splittings numerically independent.

(5) In diagrams 1—6, there are no low-slope lines allowed in $\langle 100\rangle$ and $\langle 111\rangle$ data with the same splitting. In diagrams 7—18, there is only one low-slope line in the $\langle 100\rangle$ and $\langle 111\rangle$ data with the same ZFS, and it is never the smallest ZFS. In diagrams 19—22, there are two such lines, neither of which is the smallest ZFS possible. Only in diagrams 23 and 24 does a low-slope line occur in both $\langle 100\rangle$ and $\langle 111\rangle$ data with the same ZFS which can be the smallest ZFS.

(6) The largest ZFS is not allowed in diagrams

for which the T_{2u} state is highest (diagrams 13—16, 23 and 24). It is allowed in only ⟨100⟩ data for diagrams for which the E_g state is highest (1, 2, 5, 6, 9, and 17). It is allowed in ⟨111⟩ data only if the T_{2g} state is highest (diagrams 3, 4, 10—12, and 18). It is allowed in both ⟨100⟩ and ⟨111⟩ data if the T_{1u} state is highest (diagrams 7, 8, and 19—22).

For this dipole system, we also indicate in Fig. 2 the connection of high (H) or low (L) -slope ⟨100⟩ lines to a high (h) or low (l) -slope ⟨111⟩ line through a specific ZFS. Again the five zero-field states are labled a, b, c, d, and e from top to bottom. Hence, the letters "*bd*" in the H-l quandrant of the box in diagram 1, ⟨110⟩ model, refer to the $T_{2u}-T_{2g}$ splitting as connecting a high-slope ⟨100⟩ line to a low-slope ⟨111⟩ line. The underlining of the letters "*cd*" indicates that the *cd* splitting is a ⟨111⟩ doublet (recall that there are no ⟨100⟩-allowed doublets). A transition appearing in two quadrants as in box 10, "*ad*", indicates the doublet splitting includes a high- and low-slope ⟨111⟩ line. Beside each box we include the sum rules for that diagram.

In summary, we have obtained a set of diagrams for the three simple tunneling systems that give the connections between the high-field and zero-field states and provide some detailed information about the allowed transitions for $\vec{E}_{dc}||\vec{E}_{rf}$ with $\vec{E}_{dc}||\langle 100\rangle$ or ⟨111⟩.

ACKNOWLEDGMENTS

I wish to thank F. Bridges for his encouragement and many detailed and insightful discussions. This work was supported in part by the NSF.

---

*Present address: The Center for Theology and the Natural Sciences, 2465 Le Conte Avenue, Berkeley, CA 94709.

[1]U. Kuhn and F. Lüty, Solid State Commun. 2, 281 (1964); G. Lombardo and R. O. Pohl, Phys. Rev. Lett. 15, 291 (1965).

[2]Elastic distortions, described by a stress tensor, are also associated with the impurity centers and couple to external and internal stresses. In this paper, we will focus on *paraelectric* effects, assuming that stress is not systematically and uniformly introduced into the data, and where present, produces a much smaller effect than its electric counterpart (see 10 below).

[3]Paraelectric resonance (PER) is particularly useful for investigating species with relaxation rates faster than 10^{-4} s.

[4]W. M. Kelly and F. Bridges, Phys. Rev. B 18, 4606 (1978).

[5]M. Gomez, S. P. Bowen, and J. A. Krumhansl, Phys. Rev. 153, 1009 (1967)

[6]H. B. Shore, Phys. Rev. 151, 570 (1966); P. Sauer, O. Schirmer, and J. Schneider, Phys. Status Solidi 16, 79 (1966).

[7]M. Tinkham, *Group Theory and Quantum Mechanics* (McGraw-Hill, New York, 1964).

[8]The specific dipole model (six-, eight-, or twelvefold) determines the appropriate basis for the lowered symmetry, and hence the exact characteristics of the eigenstates and energy levels at high fields.

[9]R. J. Russell and F. Bridges, following paper, Phys. Rev. B 26, 3386 (1982).

[10]Strain-allowed lines, which represent forbidden dipole transitions, may occasionally be present in a given sample due to internal strains arising from either boule or sample preparation. Typically such lines are broad and weak, and vary from sample to sample so that they can be identified in the compiled data and treated separately from the more consistent pattern of electric-dipole-allowed lines (see Ref. 14).

[11]F. Bridges, Phys. Rev. B 5, 3321 (1972).

[12]S. Kapphan, and F. Lüty, Phys. Rev. B 6, 1537 (1972).

[13]R. J. Russell, Ph. D. Thesis, University of California, 1978 (unpublished); F. Holuj and F. Bridges, Phys. Rev. B 20, 3578 (1979); F. Bridges, *ibid.* 23, 453 (1981).

[14]Several judgements must be made when interpreting data. For example, approximate degeneracies may be found between several zero-field splittings (ZFS's), both in a given field orientation and between different orientations. This may occur due to approximate degeneracies between different sets of zero-field energy levels from which these splittings arise, or due to a single transition whose value obtained by extrapolation from the data for different field orientations varies slightly. Weak lines in the data might be allowed lines which depend on small tunneling parameters, or on differences between approximately equal tunneling parameters. Alternatively, weak lines may represent forbidden electric-dipole transitions, occurring in the data from weak-strain interactions (see Ref. 10). Hence, in fitting the model to the data we must make several assumptions, assigning weak lines to allowed or forbidden transitions, and assigning approximately degenerate splittings to a single or to multiple transitions in the diagrams. Best fits for *each* set of assumptions about the data must eventual-

ly be compared before final conclusions can be stated.

[15]GBK gives several energy-level diagrams for very restricted assumptions on the relative sizes of the tunneling parameters and for a few field orientations.

[16]Normally one expects the A_{1g} eigenfunction to have the minimum energy since, having no nodes, it has the least curvature of any eigenfunction. Certainly its energy is minimized in the *two*-state systems (like NH_3) where explicit calculations show that the (single) tunneling parameter is negative. Two questions now arise: (1) With several tunneling parameters, should *all* parameters *necessarily* have negative values, and (2) whether the restriction on the sign of the tunneling parameters or the minimization of the A_{1g} energy is more strict? Preliminary results indicate that the minimization of the A_{1g} energy is less strict, allowing for *positive* values of *some* of the tunneling parameters. See Ref. 13; R. J. Russell, Bull. Am. Phys. Soc. 26, 30 (1981).

[17]In the arguments which follow, we assume the absence of accidental degeneracies in order to maximize the generality of the results. Hence, though the A_{1g} state will always be treated as having an energy no greater than any other state, other states could be degenerate with it, or with each other, in specific instances. Also, degeneracies could occur in the ZFS. The result would be that several diagrams could appear to apply equally well to the data; exact numerical solutions would then indicate which of them fits the data best.